The Maximum Radial Force of Induction Machine type Bearingless Motor using Finite Element Analysis

Akira Chiba
Science University of Tokyo, Noda, Chiba, Japan
Tadashi Fukao
Tokyo Institute of Technology, Meguro, Tokyo, Japan

ABSTRACT

Bearingless motors are high speed electric machines combined with radial magnetic bearing functions. The compactness of bearingless motors suggests the possibility of high power and high speed motors.

Four-pole electric machines with additional two-pole windings in its stator slots have been proposed by the authors. In this paper, flux distributions and radial force of a induction type bearingless motors are analyzed employing the Finite Element Method. Relationships between the radial force and radial force winding currents are also influenced by magnetic saturation. It was shown that the generated radial force reaches its maximum value due to magnetic saturation. With conventional linear controllers, experiments were found to be possible in the ranges where the radial force can be seen as a linear function. The analyzed results are confirmed with experimental results.

INTRODUCTION

High power and high speed electric drives are required for machine tools, turbo-molecular pumps, compact generators, compressors and flywheels, etc. Magnetic bearings have been employed in these high rotational speed applications [1-3]. In these applications, high power is strongly required as well as high rotational speeds.

One of the problems of magnetic bearings is that magnetic bearings occupy considerably large area. To implement magnetic bearings, a shaft length must be increased. The increased shaft length results in decreased critical speeds. Thus, it is difficult to increase rotational speeds, although control methods of flexible rotor have been investigated. In most cases, motor axial length is reduced to shorten the shaft length. In this case, it is difficult to increase output power.

Bearingless motors are high speed electric motors combined with magnetic bearing functions. The compactness of bearingless motors suggests the possibility of high power and high rotational speed motors. A disk type motor with integrated one thrust magnetic force was proposed as a bearingless motor [4]. As for bearingless motors with integrated radial magnetic forces in two radial axes, a method to unbalance line currents of conventional three-phase induction motors was proposed [5]. However, in this method, it is difficult to produce radial forces while the rotor is positioned in the center.

Four-pole electric machines with additional two-pole windings in its stator slots have been proposed by the authors [6-8]. Similar bearingless motors with four-pole windings and six-pole windings have been proposed [9-10]. Four-pole and two-pole winding configuration has advantages over other number of pole combinations in the maximum value of radial magnetic force. Principles and radial force control systems of

synchronous reluctance and induction type bearingless motors, as well as permanent magnet bearingless motors have been demonstrated [6–8]. Radial forces, voltages and currents at the additional winding terminals have been calculated based on inductance measurements. It was reported that there is an optimal exciting condition for efficient radial force production for synchronous reluctance type bearingless motors considering magnetic saturation in the previous paper [11].

However, the unbalanced four-pole flux distribution superimposed by two-pole radial force fluxes of induction type bearingless motors have not yet shown. The non-linear radial force functions with respect to the radial force winding current have not made clear. The maximum radial force, which can not be achieved in simple experiment systems, has not yet reported.

In this paper, the influence of magnetic saturation of radial forces is calculated by the Finite Element Method. The four-pole flux distributions superimposed with two-pole radial force fluxes are shown. As radial force winding current increases, radial force is found to be saturated. The calculated results were compared with measured radial forces. Experiments were possible in the range where the radial force can be approximated as a linear function. The maximum radial force achieved in experiments is about 70% of the theoretical value.

RADIAL FORCE

FIGURE 1 shows principles of radial force production of the proposed bearingless motors. The stator has four-pole motor windings N_a and N_b as well as two-pole radial force windings N_α and N_β. With the current in the motor winding N_a, four-pole revolving field Ψ_4 is produced. In addition to the four-pole magnetic field, the two-pole fluxes Ψ_2 are produced by the current of the two-pole windings N_β. As shown in the FIGURE 1, the flux density in B_+ increases but B_- decreases. Radial force is generated in β-axis. With negative current in the N_β winding, radial force can be produced in opposite direction. The current in the N_α winding produces radial force in the α-axis. In this principle, the amplitude and the direction of the radial force can be controlled by the amplitude and phase shift in the two-pole winding currents.

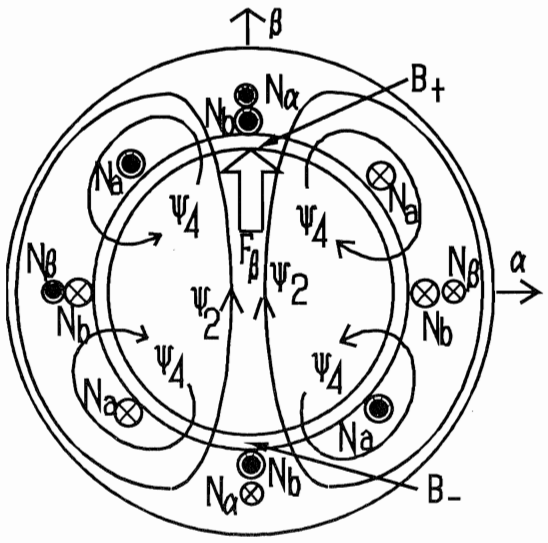

FIGURE 1:Radial Force Production

FIGURE 2 shows system configuration for a induction type bearingless motor with two radial axis position controls. Radial positions α and β are detected by eddy current type sensors. These displacements are compared with radial position references α^* and β^*, then, position errors are generated. Radial force commands F_α^* and F_β^* are generated with radial position controllers. Radial force winding currents i_α^* and i_β^* are generated in accordance with the direction ϕ, i.e., the angle of the revolving magnetic field. The weight is prepared to apply steadily radial force to the shaft. Even though steadily radial force is applied, radial positions are to follow the reference values with integrating functions of radial position controllers.

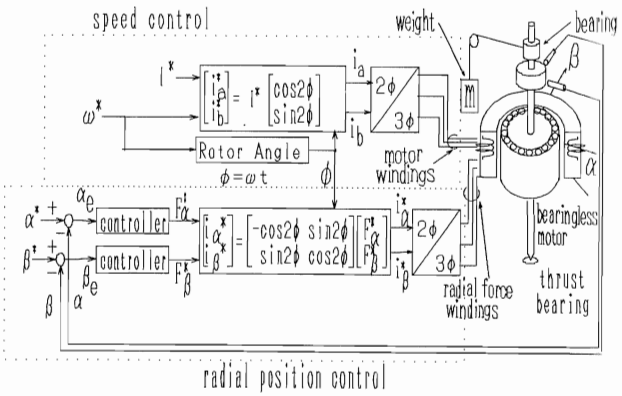

FIGURE 2:System Configuration

SYSTEM

The motor winding currents are supplied so that no load operations of the induction motor are possible with a constant exciting current at variable speeds.

MACHINE MODEL

FIGURE 3 shows the winding configuration of a prototype bearingless motor. The stator has two sets of three-phase windings although two-phase windings were shown in FIGURE 1 for simplicity. Four-pole windings are wound as motor windings. Two-pole windings are for radial force generation. Number of turns in each slot is 48 and 36 for four-pole and two-pole windings, respectively. All conductors are with a diameter of 0.6mmϕ and in series. The stator outer and inner diameters are 90mm and 49mm, respectively. The stack length of stator and rotor irons is 30.8mm. Iron cores are made of laminated silicon steel in 0.5mm thickness. The rotor outer diameter is 48.25mm. Search coils are wound in two stator teeth to measure tooth flux densities. The output voltage of the search coils are integrated and peak flux densities can be measured.

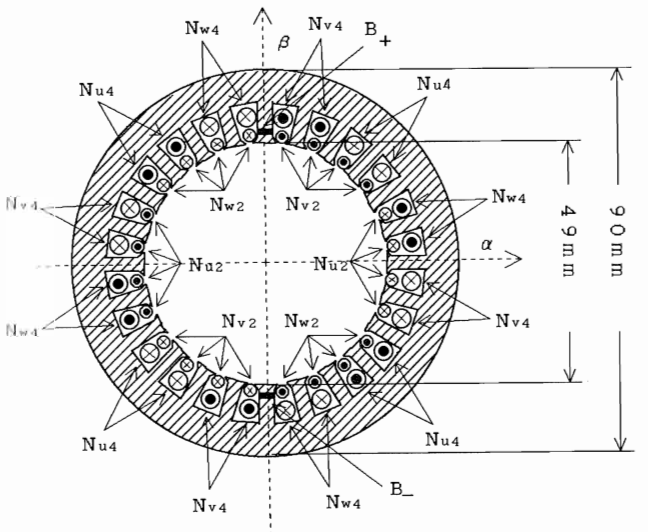

FIGURE 3:Machine Model

FEM RESULTS

FIGURE 4 shows nodes and elements for FEM analysis. There are 5136 elements and 2617 nodes. Cage bars in the rotor are neglected to avoid influence of space harmonics because the rotor of the test machine is skewed. Rotor shaft space is also neglected for simplicity in the FEM model.

Sinusoidal balanced currents are supposed in the FEM analysis. The analysis was done when the current of u-phase windings N_{u4} and N_{u2} are peak values. The other windings hold the half value of those peak currents. The rotor is assumed to be in the center position.

FIGURES 5(a)-(d) show the flux distributions. The current of radial force windings are zero in FIGURE 5(a). Four-pole balanced flux distribution can be seen. Produced radial force is zero. The tooth flux density B_+ and B_- are both equal to 0.9T. The air-gap flux densities are about 0.4T.

When the radial force winding current is increased, two-pole flux distribution is superimposed. The radial force is generated in FIGURE 5(b). It can be seen that the tooth flux density B_+ is increased to 1.2T and B_- is decreased to 0.8T. This unbalanced flux density distribution results in radial force of 6kgf. The radial force was calculated by integrating forces along the air-gap.

As the radial force winding current increases, the flux density B_- is decreased to almost zero as shown in FIGURE 5(c). If the radial force winding current is increased beyond this point, the flux density B_- changes its direction. The flux distribution looks like two-pole machines rather than four-pole machines. Thus, magnetic forces of rotor elements around B_- increases, which results in a reduction in radial force. The derivative of the radial force with respect to the radial force winding current decreases beyond this point.

On the contrary, flux density B_+ is saturated. As a result, the radial force reaches its maximum value as shown in FIGURE 5(d). If the radial force winding current is increased beyond this point, B_+ is saturated, B_- is increased and radial force is decreased as shown in FIGURE 5(e).

FIGURES 6(a)-(d) shows flux density distribution along the air-gap. These figures (a)-(d) are corresponding to FIGURES 5(a)-(d). In FIGURE 6(a), four-pole symmetrical flux distributions are seen. The flux distributions include space harmonics caused by stator teeth. In FIGURE 6(b), flux density increased around ϕ=90deg, which corresponds to the B_+ tooth.

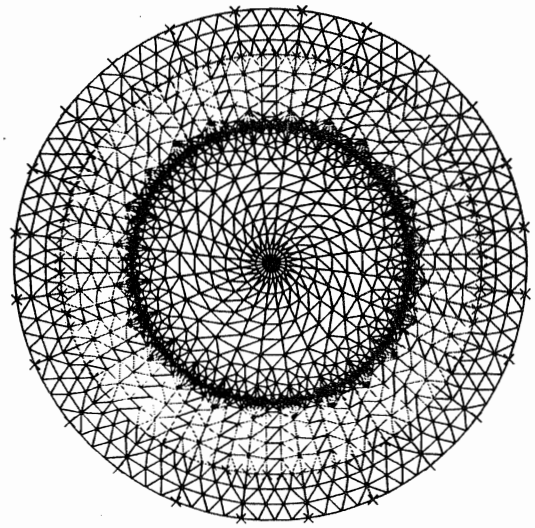

FIGURE 4:Nodes and Elements

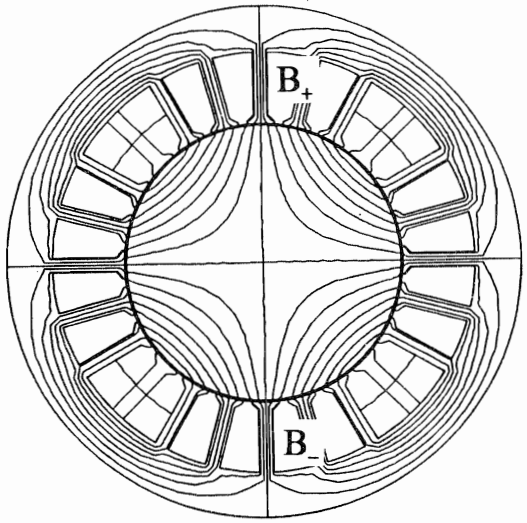

(a)I_2=0A

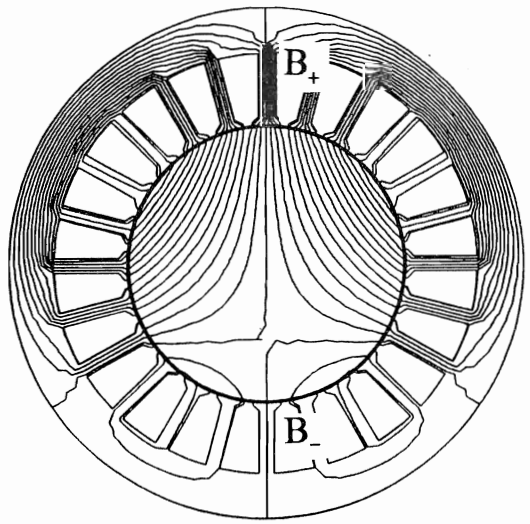

(b)I_2=0.5A

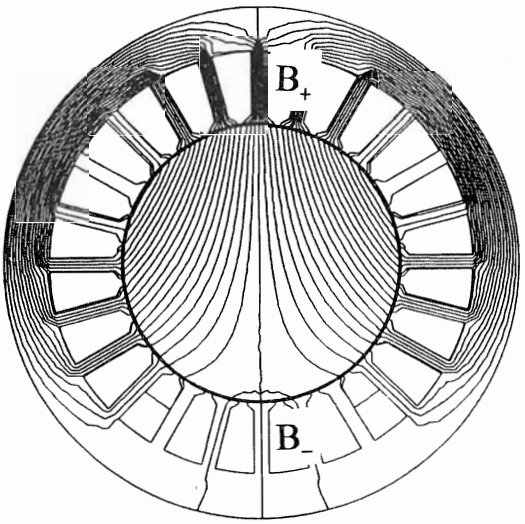

(c)I_2=0.8A

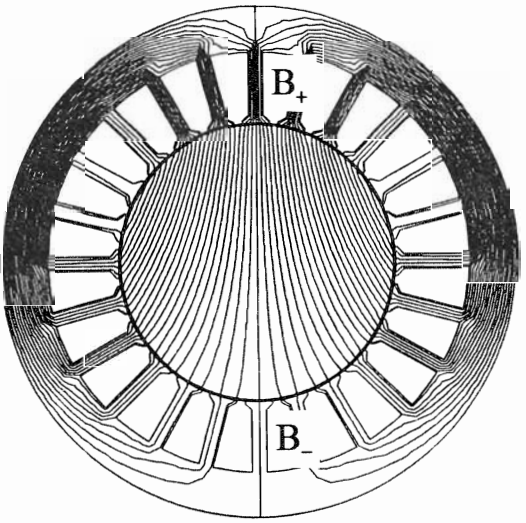

(d)I_2=1.2A

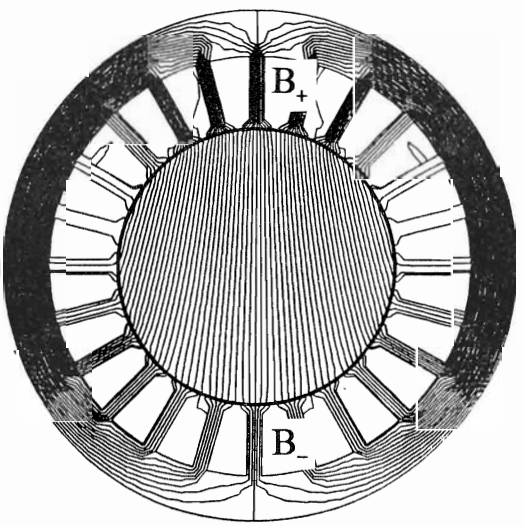

(e)I_2=2.5A

FIGURE 5:Flux Distributions

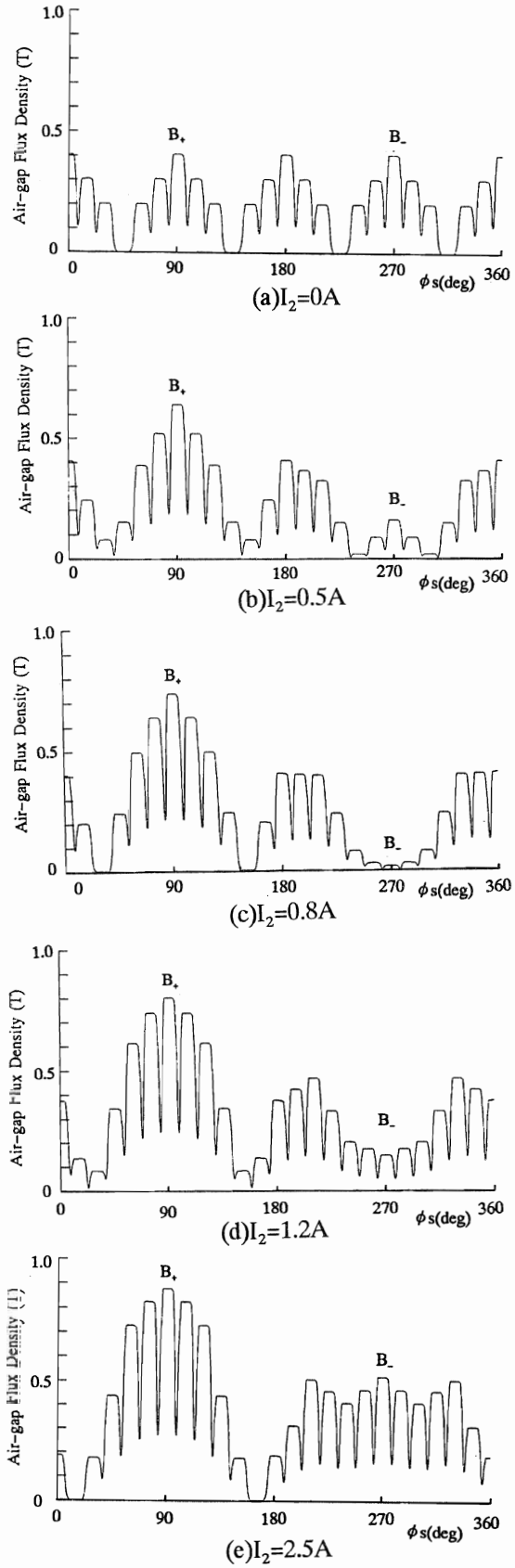

FIGURE 6:Flux Density Distribution

However, the flux density is decreased around ϕ=270 deg, i.e., the B_ tooth. FIGURES 6(a)–(e) show the flux densities in the air–gap, but not tooth flux densities.

In FIGURE 6(c), B_ is decreased to almost zero. The flux density B_+ is saturated because of serious magnetic saturation in stator teeth. In FIGURES 6(d) and (e), B_ is increased in opposite direction.

COMPARISONS

FIGURE 7 shows the tooth flux density variations with respect to the radial force winding current. The flux density in low side B_ decreases as the radial force winding current increases. The operating points **a**, **b**, **c**, **d** and **e** are corresponding to the flux distributions in FIGURES 5(a)–(e) and FIGURES 6(a)–(e), respectively. The opposite direction flux density in B_ is plotted in negative values in FIGURE 7.

FIGURE 8 shows the radial force as a function of radial force winding current. The curved line shows the calculated values by FEM program. The measured operating points are also shown. It is seen that the radial force increases linearly as radial force winding current increases only at low current.

The radial force is saturated beyond operating point **c**. At this point, the tooth flux density B_ is zero as seen in FIGURE 7. Then, the radial force is saturated and reaches the maximum value at operating point **d**. The tooth flux density B_+ is saturated and B_ is increased in opposite direction as seen in FIGURE 7. The radial force is decreased over the maximum value even though radial force current is increased. Experiments were possible when the radial force can be seen as a linear function. It is also found that the maximum value achieved in the experiments is almost 70% of the theoretical value.

CONCLUSION

In this paper, the flux distributions are analyzed by the Finite Element Method. The radial force is calculated from the flux distribution. The radial force is not a linear function at high radial force winding current. The radial force is saturated and reaches its maximum value. The experiments were found to be possible up to 70% of the theoretical value due to the non–linear characteristics.

In order to derive the maximum radial force, motor

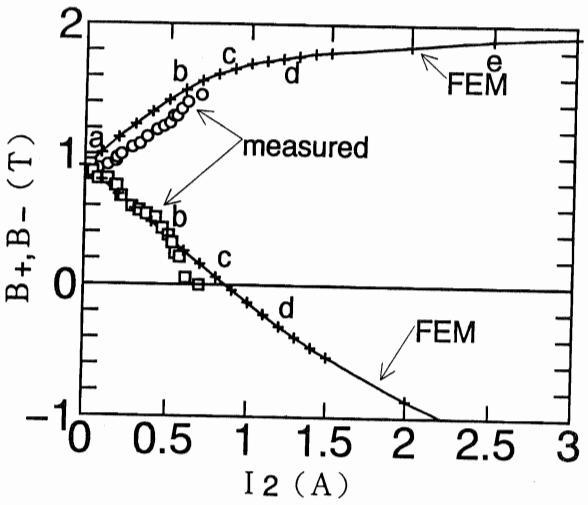

FIGURE 7:Flux Densities

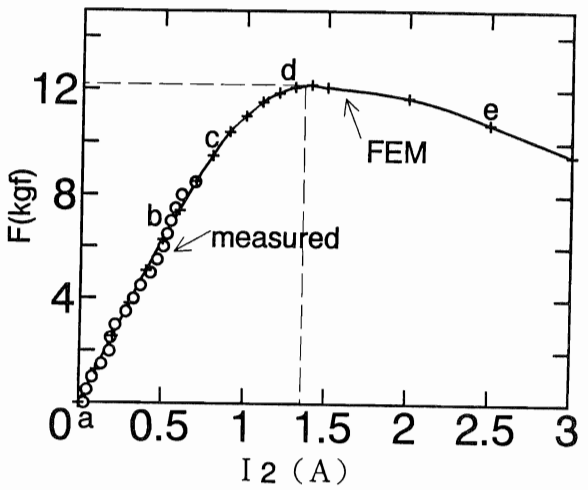

FIGURE 8:Radial Force and Current

exciting conditions will be investigated in the future.

REFERENCES

[1] M.Ota,etal.,"Monitoring and Actuating Function of the Internal Grinding Spindle with Magnetic Bearing", Proc. of 2nd International Symposium on Magnetic Bearing, pp.27-32,1990, Tokyo

[2] Michel Dussaux,"The Industrial Applications of the Active Magnetic Bearings Technology", Proc. of 2nd International Symposium on Magnetic Bearing, 1990 , pp.33-38

[3] M.Brunet,"Practical Applications of the Active Magnetic Bearings to the Industrial World", Proc. of 1st International Symposium on Magnetic Bearing, pp.225-244, 1988

[4] Bosch, R.,"Development of a Bearingless Electric Motor", Proc. of ICEM'88, vol.3, pp.331-335

[5]A.O.Salazar,etal.,"A Magnetic Bearing System using Capacitive Sensors for Position Measurement", IEEE Trans. Magnetics, MAG-26, no.5, 2541, 1990

[6] A.Chiba, etal.,"Principle and Characteristics of a Reluctance Motor with Windings of Magnetic Bearing", IPEC'90-Tokyo, pp.919-926, 1990

[7] A.Chiba, etal.,"No Load Characteristics of a Bearingless Induction Motor", IEEE IAS Annual Meeting Conference Record, pp.126-132, 1991

[8] M.Oshima, etal.,"Characteristics of a Permanent Magnet Type Bearingless Motor", IEEE IAS Annual Meeting Conference Record, 1994 (to be presented)

[9] J.Bichsel,"The Bearingless Electrical Machine", NASA-CP-3152-PT-2, pp.561-573, 1992

[10] Y.Okada, etal.,"Analysis and Control of a Permanent Magnet Type Levitated Rotating Motor", IEEJ Proc. of Symposium on Dynamics of Electro Magnetic Force, pp.251-256, 1992 (written in Japanese)

[11] A.Chiba, etal.,"Effects of Magnetic Saturation on radial Force of Bearingless Synchronous Reluctance Machines",IEEE IAS Annual Meeting, vol.3, pp.233-239, 93CH3366-2, 1993